Journal of Highway and Transportation Research and Development
2024,18(1):27-37
ISSN 2095-6215
DOI: 10.26599/HTRD.2024.9480004

Development of Battery Electric Vehicle's Driving Cycle in the Mountain Environment Based on Big Data

Shujiang Zhu*[1], Tingting Xu[2], Fangjia Long[2], Xiaorui Hu[2]

(1. China Automotive Engineering Research Institute Co., Ltd., Chongqing 401122, China;
2. State Grid Chongqing Electric Power Company, Chongqing 400015, China)

Abstract: With the increasing trend of battery electric vehicles, it is no longer appropriate to use the traditional fuel vehicle's driving cycle for battery electric vehicle driving cycle research. In order to obtain the driving cycle of the battery electric vehicle and compare it with the traditional driving cycle from a data perspective, the driving data of the battery electric vehicle in the Chongqing area was analyzed. The proprietary big data platform provided whole vehicle and battery data, and the short-stroke method was used to identify the kinematic fragments. Then, the kinematic fragments' feature is constructed using the correlation method of feature engineering. The dimension of high-dimensional feature data is reduced through principal component analysis, and the feature weight is calculated to eliminate the influence of feature correlation. Next, the K-means++ clustering method is used to partition the structure of the driving speed and battery current curves, and thus to construct four types of working conditions: low speed, medium speed, medium-high speed, and high speed. Moreover, the most suitable short-time working conditions are selected by sorting the distance of each working condition from the cluster center as the origin. The weight of the data set is determined by the ratio of the total duration of the data set to the total duration of the data set. Through error analysis, the characteristic deviation error of the smallest curve is selected as a representative of the working condition to determine the representative of the vehicle and battery working conditions. Finally, the reliability of the battery electric vehicle operating curve in a mountainous environment is demonstrated by comparing international and domestic typical operating conditions. The results indicate that in mountainous environments, pure electric vehicles exhibit shorter constant speed driving times, longer idling times, greater deceleration, and a smaller proportion of deceleration time compared to non-mountainous environments. Additionally, battery discharge efficiency is higher, and the vehicle speed is maintained at a moderate level.

Key words: automotive engineering; driving cycle; principal component analysis; kinematic fragment; Kmeans++ clustering analysis; battery electric vehicle; mountain environment

0 Introduction

Vehicle driving cycle is the description of the velocity-time relationship in the process of vehicle driving[1]. The study of vehicle driving cycle in different regions can reflect the impact of different landforms, environments and cities on vehicle driving.

In the early research of China's driving cycle, New European Driving Cycle (NEDC) was introduced to analyze and certify China's automobiles[2]. As the number of cars in China continues to increase, the impact of China's diverse geographical environment and vehicle models on vehicle driving is becoming more and more obvious, and the deviation of NEDC from the description of driving cycle in China is also becoming more and more obvious. In response to this problem, a large number of scholars have carried out a lot of research in combination with different geographical environments and vehicle models, and introduced new driving cycles.

CAI E et al. constructed the vehicle driving cycle in Xi'an based on the vehicle data in Xi'an[3]; XU Ting et al. collected the test vehicle data of the G318 Sichuan-Tibet Highway, and used the Markov chain method to construct the driving cycle of passenger vehicles in plateau mountainous areas[4]; Sun Jun et al. used the public transport data in Hefei to cluster and constructed electric bus driving cycle[5]; LIU Yu et al. collected passenger vehicle data in 41 cities, and used weighted combination

Received 2 September 2023; Revised 28 November 2023; Accepted 5 January 2024

* *E-mail address*: 695699484@qq.com

to construct the China passenger vehicle driving cycle[6], as an important part of the "China working condition"[7]; TONG added vehicle power characteristics when developing the Hong Kong electric bus driving cycle[8]; HU Zheng-yun used segment division and Monte Carlo simulation optimization methods to construct. The high-precision passenger car driving cycle in Xi'an[9]; WANG Wen-qi used the sliding window method to idling the motion segments, divided into three optimal segment types, and constructed the driving cycle[10]; HU Zhi-yuan et al. used 10 vehicles Based on the driving data of 12 consecutive months, the driving cycle based on a large sample of passenger car in Shanghai is constructed[11].

According to data from the China Automobile Association, the national production and sales of new energy vehicles in China in 2019 and 2020 are both above 1 million, and it is expected to reach 2.8 million in 2026[12]. With the development of new energy vehicles, the significance of developing new energy vehicle driving cycles is becoming increasingly important. YU Man et al. used a semi-supervised learning method combining mean clustering and SVM to construct the Xi'an electric vehicle driving cycle[13]; QUE Hai-xia et al. used a variety of methods to develop driving cycle of electric vehicles in Xi'an[14]; LI Yao-hua et al. classified Xi'an electric city buses, and analyzed three typical driving cycles[15]; XU Xiao-jun found that there are obvious differences in the cycles by comparing the driving cycles of electric vehicles and traditional vehicles respectively[16]; PAN Deng constructed the driving cycles of plug-in hybrid electric vehicles based on kinematic and statistical characteristics[17]. Up to now, the research on the driving cycles of new energy vehicles, especially pure electric vehicles(PEV), is relatively shallow, mainly limited to the small amount of data, and the data characteristics still consider the characteristics of traditional vehicles.

In this paper, after optimizing the idle segment and parking interval, the motion segment is extracted, and based on the vehicle velocity feature, the battery feature is added to build a feature library, and the PCA dimension reduction, K-means++ clustering, weighted combination and other methods are used to construct the driving cycle including velocity and current. The driving cycles of PEV are compared and analyzed to reflect the real driving cycles of PEV in the mountainous environment of Chongqing.

1 Construction of driving cycle

Using the self-built new energy vehicle national monitoring and management platform Southwest Branch Center Big Data Analysis Platform (hereinafter referred to as the Southwest Branch Center Big Data Platform), collecting pure electric vehicle driving data per second, the development process of pure electric vehicle driving cycle is shown in Figure 1. First, data preprocessing is performed on the collected data, and then the cleaned data is divided into kinematic segments, and the kinematic segments are used as statistical units to extract features, and the constructed features are processed into principal component analysis to achieve the purpose of feature reduction, and then perform the cluster analysis on kinematic segments, synthesize candidate driving cycles according to the clustering results, and finally verify the error of the candidate driving cycles, and screen out the final driving cycle curve output with the smallest error.

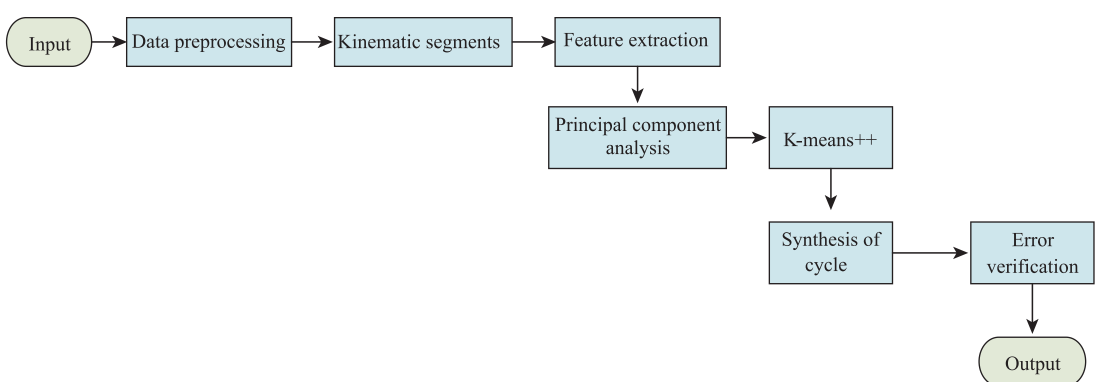

Fig. 1 Driving cycle development process

1.1 Data collection and data preprocessing

Chongqing is a typical mountain city, with more than 75% of the mountainous area and 20% of the land with a slope of more than 25 degrees. Through the big data platform of the Southwest Branch Center, the driving data of the test pure electric vehicle in Chongqing area from August 16, 2020 to February 7, 2021, as well as the driving data of the same model in Beijing area during the same period, were collected. The time interval for data collection is 1 second, including parameters such as time, mileage, velocity, latitude, longitude, and current.

Due to the influence of factors such as environmental changes and equipment errors, there are some abnormal values in the collected data, which need to be preprocessed before they can be used. The velocity screening steps are as follows:

(1) Delete the data items that are obviously abnormal. Such as time repetition, abnormal longitude and latitude, abnormal velocity, abnormal acceleration and other problems.

(2) Linear interpolation fills in missing data. Considering that the larger the time interval is, the more complicated the driving situation of the car is, only the data missing 1 second is filled with linear interpolation.

(3) Idle abnormal processing. For a long-term driving situation where the vehicle velocity is less than 10 km/h and not all 0, it is treated as an idling abnormality, and only the driving data of the first 180 are retained.

(4) Handling of parking exceptions. For the long-term driving situation where the vehicle velocity is 0, it is treated as a parking abnormality, and only the data of the first 5 s and the last 5 s are retained as the starting and parking stages for subsequent analysis.

The amount of data before and after data processing is compared in Table 1. The first 2 000 s of data after data preprocessing are taken, and the velocity-time curve is drawn as shown in Figure 2.

1.2 Feature construction of kinematic segments

1.2.1 Division of kinematic segments

A kinematic segment refers to a segment of driving data that includes the four motion states of the car: uniform velocity, acceleration, deceleration, and idle velocity[18]. The best way to divide kinematic segments is that starting point is the start of the idle state, and the end point is the moment before the next idle state starts. The schematic diagram of the kinematic segment is shown in Figure 3.

Table 1 Quantity comparison before and after data preprocessing

Begins	Number of data after removing	Number of data after filling	Handle abnormal idling and post-stop data volume
949 601	947 181	947 424	350 207

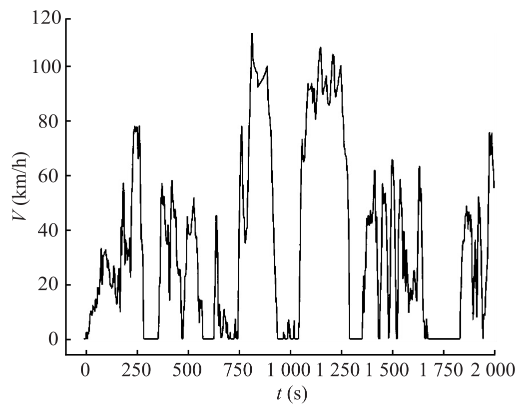

Fig. 2 Velocity-time graph

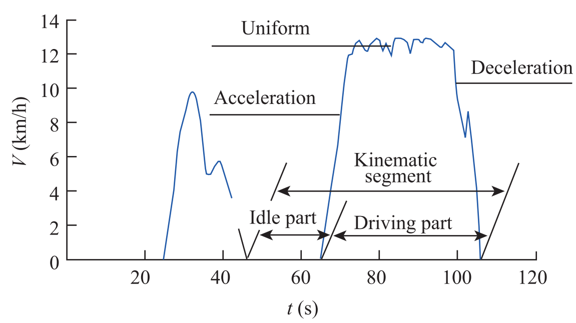

Fig. 3 Schematic diagram of kinematics fragments

According to the definition of kinematic segments, the pre-processed data is divided into multiple candidate segments. In order to improve the representativeness of the kinematic segments to the actual driving situation, the candidate kinematic segments need to be screened, and only the segments with a duration greater than 20 s and kinematic segments with an intra-segment time missing rate of less than 10% and an intra-segment time missing no more than 10 s. The comparison of the number of kinematic fragments before and after screening is shown in Table 2.

Table 2 Comparison of the number of kinematic fragments before and after screening

Number of candidate	Number of clips after the deletion time is less than 20 s	Number of clips after the deletion time is greater than 10%	Number of clips after the deletion time exceeds 10 s
1 422	1 398	1 233	1 161

1.2.2 Kinematic segment features

Treating kinematic segments as statistical units, kinematic segment features are extracted from three aspects: kinematic features, battery operating features, and statistical features. A total of 30 features are extracted as shown in Table 3.

Table 3 Feature of kinematics fragments

Param	Explanation	Unit	Calculation method
T	Total time	s	Count the total time
S	Total distance	m	Average velocity of adjacent data within a segment is multiplied by the time interval and added up
T_i	Idle time proportion	—	Idle duration/T
T_a	Acceleration time proportion	—	Acceleration duration/T
T_d	Deceleration time proportion	—	Deceleration duration/T
T_e	Uniform time proportion	—	Uniform duration/T
V_{max}	Maximum velocity	km/h	$\max\{v_1, v_2, v_3, \cdots\}$, $v_1, v_2, v_3, \cdots$ is velocity
V_m	Average velocity	km/h	$\text{mean}(v_1, v_2, v_3, \cdots)$
V_{mr}	Average running velocity	km/h	Accumulation of vehicle velocity/number of data in the running section
V_s	Standard deviation of velocity	km/h	$\text{std}(v_1, v_2, v_3, \cdots)$
A_{max}	Maximum acceleration	m/s^2	$\max\{a_1, a_2, a_3, \cdots\}$, $a_1, a_2, a_3, \cdots$ is acceleration
A_m	Average acceleration	m/s^2	$\text{mean}(a_1, a_2, a_3, \cdots)$
A_s	Standard deviation of acceleration	m/s^2	$\text{std}(a_1, a_2, a_3, \cdots)$
D_{max}	Maximum deceleration	m/s^2	$\max\{d_1, d_2, d_3, \cdots\}$, $d_1, d_2, d_3, \cdots$ is deceleration
D_m	Average deceleration	m/s^2	$\text{mean}(d_1, d_2, d_3, \cdots)$
D_s	Standard deviation of deceleration	m/s^2	$\text{std}(d_1, d_2, d_3, \cdots)$
T_f	Discharge time proportion	—	Duration of forward current/T
T_b	Energy recovery time proportion	—	Duration of backward current/T
I_{fmax}	Maximum discharge current	A	$\max\{i_1, i_2, i_3, \cdots\}$, $i_1, i_2, i_3, \cdots$ is discharge current
I_{fm}	Average discharge current	A	$\text{mean}(i_1, i_2, i_3, \cdots)$
I_{fs}	Standard deviation of discharge current	A	$\text{std}(i_1, i_2, i_3, \cdots)$
Ib_{max}	Maximum energy recovery current	A	$\max\{ib_1, ib_2, ib_3, \cdots\}$, $ib_1, ib_2, ib_3, \cdots$ is energy recovery current
Ib_m	Average energy recovery current	A	$\text{mean}(ib_1, ib_2, ib_3, \cdots)$
Ib_s	Standard deviation of energy recovery current	A	$\text{mtd}(ib_1, ib_2, ib_3, \cdots)$
Ia_{max}	Maximum acceleration of discharge current	A/s	$\max\{ia_1, ia_2, ia_3, \cdots\}$, $ia_1, ia_2, ia_3, \cdots$ is acceleration of discharge current
Ia_m	Average acceleration of discharge current	A/s	$\text{mean}(ia_1, ia_2, ia_3, \cdots)$
Ia_s	Standard deviation of discharge current acceleration	A/s	$\text{std}(ia_1, ia_2, ia_3, \cdots)$
Id_{max}	Maximum deceleration of energy recovery current	A/s	$\max\{id_1, id_2, id_3, \cdots\}$, $id_1, id_2, id_3, \cdots$ is deceleration of energy recovery current
Id_m	Average deceleration of energy recovery current	A/s	$\text{mean}(id_1, id_2, id_3, \cdots)$
Id_s	Standard deviation of energy recovery current deceleration	A/s	$\text{std}(id_1, id_2, id_3, \cdots)$

The above features are calculated for each kinematic segment, and the calculation results of the first 15 features of some motion segments are shown in Table 4.

Table 4 Part of calculate results of kinematics fragments

No.	T	S	T_i	T_a	T_d	T_e	V_{max}	V_m	V_{mr}	V_s	A_{max}	A_m	A_s	D_{max}	D_m
1	140	801.93	0.05	0.31	0.4	0.24	33.2	20.55	21.14	6.97	1.33	0.43	0.28	1.52	0.32
2	113	1 538.64	0.01	0.44	0.44	0.11	77.9	48.69	49.04	19.75	2.75	0.83	0.65	2.08	0.81
3	184	1 144.19	0.41	0.24	0.31	0.04	58	22.30	37.40	20.76	2.80	0.69	0.61	2.5	0.52
4	255	3 887	0.26	0.23	0.30	0.21	111.7	54.70	73.64	39.17	2.16	0.72	0.48	1.69	0.54
⋮	⋮	⋮	⋮	⋮	⋮	⋮	⋮	⋮	⋮	⋮	⋮	⋮	⋮	⋮	⋮

1.3 Feature dimension reduction and K-means++ clustering

1.3.1 PCA feature dimension reduction

This paper selects 12 feature indicators and 4 statistical indicators related to the vehicle motion, and 12 feature indicators and 2 statistical indicators related to battery operation. There are 30 indicators in total. The feature dimension is high, and the correlation coefficient matrix between features is shown in Figure 4, which indicates that some features have a certain correlation, so it is considered to reduce the feature dimension. In this paper, the PCA principal component analysis method is used to reduce the dimension of the features, and the specific steps are shown in Figure 5.

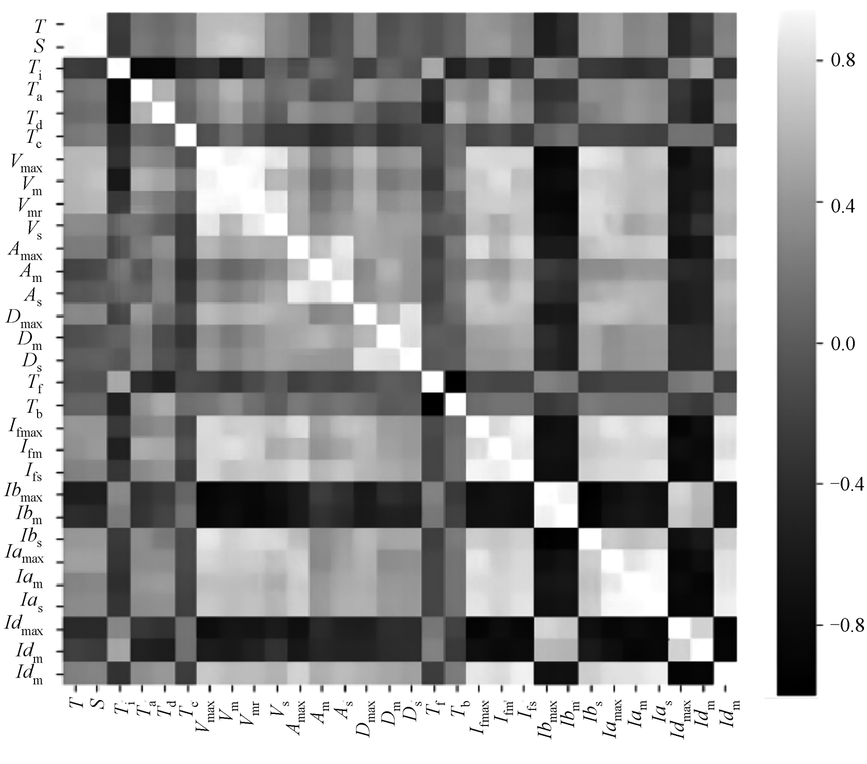

Fig. 4 Correlation coefficient matrix of kinematics segment features

The variance contribution rate of the top 6 principal components is calculated to reach 87%, and the variance contribution rate of each principal component is shown in Table 5. Therefore, the top 6 principal components are taken in this paper, and each kinematic segment is composed of a new 6-dimensional vector represented, as shown in Table 6.

1.3.2 K-means++ clustering

The K-means algorithm is the most commonly used unsupervised clustering algorithm. It is necessary to determine the hyperparameter K value of the cluster and randomly initialize the centroid, and continuously update the centroid according to the distance calculation formula until convergence. The initial centroid selection of the K-

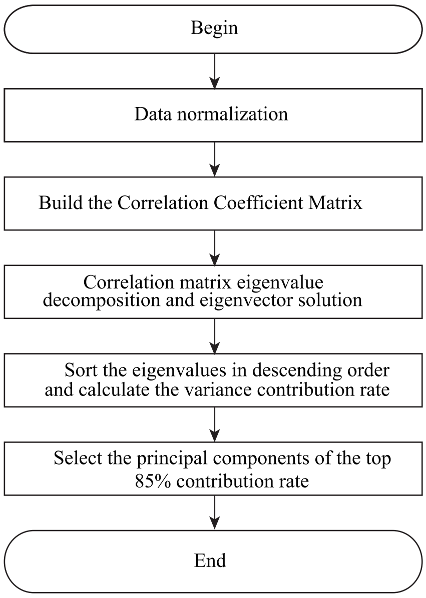

Fig. 5 Principal component analysis steps

Table 5 Variance contribution rate of each principal component

Principal component	$P1$	$P2$	$P3$	$P4$	$P5$	$P6$	⋯
Variance contribution rate(%)	51.62	12.65	9.89	5.69	4.86	2.93	⋯
Cumulative contribution rate(%)	51.62	64.27	74.16	79.85	84.71	87.64	⋯

Table 6 Principal component eigenvalues of partial kinematics segments

Kinematic segment	$P1$	$P2$	$P3$	$P4$	$P5$	$P6$
1	−3.58	−1.828	−0.18	−0.33	−0.45	1.25
2	4.92	−0.07	−1.25	0.28	0.35	0.16
3	1.35	2.22	0.26	−1.47	1.35	0.81
⋮	⋮	⋮	⋮	⋮	⋮	⋮
1 161	3.05	−1.43	−0.15	−0.20	0.81	−1.05

means algorithm is random, which has a great impact on the final clustering results and the running time of the clustering algorithm. The K-means++ clustering method improves the initial value selection method of the K-means algorithm. The steps of the K-means++ algorithm are as follows:

(1) Determine the K value of the cluster number of clusters;

(2) Randomly select a data point as the first centroid;

(3) For each remaining data point, calculate the minimum Euclidean distance from the determined centroid:

$$d(x_i) = \min \| x_i - \mu_s \|_2^2,\ s = 1,2,\cdots,K_{\text{selected}} \quad (1)$$

(4) Weight the remaining data points according to $d(x_i)$ to determine a new centroid;

(5) Steps (3) and (4) are repeated until k centroids are determined;

(6) K-means clustering is performed using the k centroids as initialized centroids.

For the determination of the hyperparameter k value, this paper uses the silhouette coefficient and the SSE (intra-group sum of squares error) elbow method to select. The silhouette coefficient figure and SSE distribution figure are shown in Figure 6. The abscissas of the left and right subgraphs represent the number of clusters, the ordinate of the left represents the average value of the sample Silhouette score, and the ordinate of the right represents the sum of squares of errors within the sample group. The selection principle is that the larger the silhouette coefficient, the smaller the SSE value, and the moderate number of clusters. Combined with the silhouette coefficient and SSE results, 5 clusters are preferen-

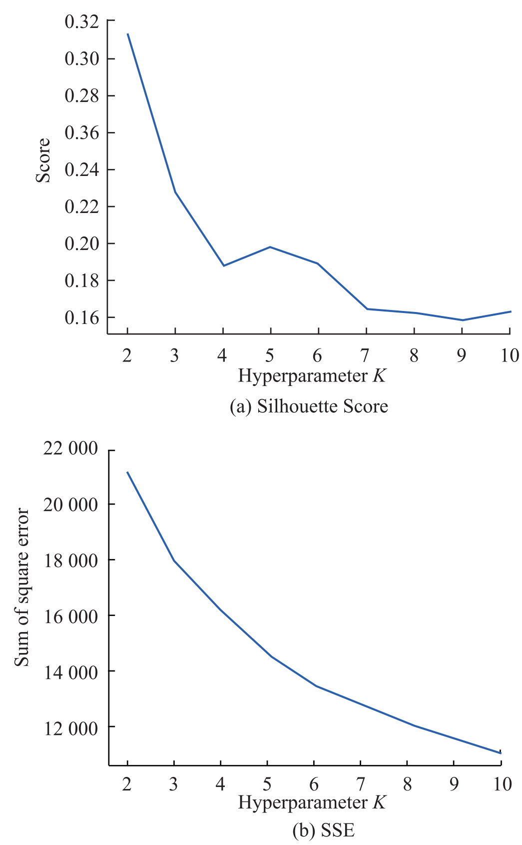

Fig. 6 Silhouette Coefficient Distribution & SSE Distribution

tially selected to cluster the sample data. However, in the actual calculation, among the 5 types of kinematic segment, one type of segment does not meet the time requirement, and thus degenerates into 4 clusters. Take $K=4$ for K-means++ clustering. Considering that the features of the maximum type are not suitable for mean value processing, only 21 eigenvalues are taken, and the cluster centers are shown in Table 7.

Table 7 K-means++ cluster center

	Cluster1	Cluster2	Cluster3	Cluster4
T_i	0.55	0.13	0.15	0.07
T_a	0.20	0.36	0.37	0.40
T_d	0.17	0.34	0.34	0.37
T_e	0.08	0.17	0.14	0.16
V_m	12.13	22.89	35.08	53.68
V_{mr}	24.60	25.73	40.88	57.44
V_s	13.51	12.12	20.51	25.30
A_m	0.54	0.45	0.55	0.57
A_s	0.38	0.31	0.41	0.47
D_m	0.53	0.44	0.58	0.62
D_s	0.42	0.34	0.47	0.51
T_f	0.85	0.67	0.69	0.69
T_b	0.13	0.31	0.30	0.30
I_{fm}	11.12	18.93	32.99	52.73
I_{fs}	16.14	18.61	31.49	46.17
I_{bm}	−9.75	−9.46	−20.28	−30.34
I_{bs}	10.13	9.19	16.16	23.38
IA_m	6.25	8.18	15.03	25.26
IA_s	9.45	10.59	19.23	30.74
ID_m	−5.60	−10.42	−18.16	−28.98
ID_s	11.28	13.68	24.08	36.42

Analyzing the features in different clusters in Table 7, it can be found that: The idle time proportion of kinematic segments and the discharge time proportion of the first category is much higher than that of the other three categories, but the average velocity, average running velocity, and energy recovery time proportion and the average discharge current are smaller than the other three types. Combining these indicators, the motion features of PEV described in the first type of kinematics segment can be obtained: the vehicle runs at a low velocity and is in a waiting state for a long time. The first type of motion segment describes the low-velocity driving cycle of the car in the case of traffic jams.

The kinematic segments of the second category are basically consistent with the third category, and also are similar to the fourth category in the 6 indicators of idle time proportion, acceleration time proportion, deceleration time proportion, uniform time proportion, discharge time proportion, energy recovery time proportion. But the average velocity, average running velocity, velocity standard deviation, average acceleration, acceleration standard deviation, average deceleration, deceleration standard deviation, and battery-related indicators are all smaller than the third and fourth categories. Combining these indicators, the motion features of PEV described by the second type of kinematic segment can be obtained: the vehicle travels at a low velocity, but does not encounter a lot of congestion. The second type of kinematic segment describes the safe, medium and low velocity driving cycle of the car on a smooth road, but the velocity is lower, which is more related to the user's driving habits and pays more attention to safety.

The idle time proportion of the third type of kinematic segment is twice that of the fourth type, and the rest of the indicators are smaller than the fourth type. Combining these indicators, the motion characteristics of the pure electric vehicle described by the third type of kinematic segment can be obtained: the velocity is moderate and traffic is smoother. The third type of kinematic segment is similar to the second type of motion segment, which describes the medium and high-velocity driving conditions of the car in the urban area with smooth roads.

The idle time proportion of the fourth type of kinematic segment is the smallest among the four types of kinematic segments, which is only 0.07, and the other indicators are the maximum values among the four types of kinematic segments. Combining these indicators, the motion features of PEV described in the fourth category of kinematic segments can be obtained: the vehicle travels at a high speed and rarely encounters congestion. The fourth type of kinematic segment describes the high-speed driving cycle of the car in the suburbs or highways, and the vehicle is in a high-speed driving state for a long time.

1.4 Synthesis and verification of candidate working conditions

1.4.1 Extraction and splicing of motion segments

Referring to NEDC, WLTC and China's CATC, and considering the integrity of kinematic segments, the driving cycle duration of PEV is limited to 1 500 - 2 300 s. The time range of various cluster fragments is calculated as shown in formula (2):

$$T_k = T_{\text{total}} \times \frac{\sum_{i=1}^{m} t_{i,k}}{\sum_{k=1}^{K}\sum_{i=1}^{m} t_{i,k}}, \tag{2}$$

where, T_k is the duration of the k-th kinematic segment in the candidate cycle; T_{total} is the total duration of the final cycle; and $t_{i,k}$ is the i-th segment duration of the k-th type of kinematic segment.

Substituting T_{total} equal to 1 500 s and 2 300 s into formula (2) can calculate the duration range of various segments that meet the duration requirements, among which the duration of low-speed segments is from 173 s to 266 s, the duration of medium-low-speed segments is from 267 s to 410 s, and the duration of medium-high-speed segments is from 575 s to 880 s, the high-speed segment duration is from 485 s to 744 s, and the distance between each type of cluster and this type of centroid is calculated. The distance formula is calculated by formula (3).

$$d_{i,k} = \| x_{i,k} - \mu_k \|, \tag{3}$$

where, $d_{i,k}$ is the distance from the i-th segment of the k-th type of kinematic segment to the centroid; $x_{i,k}$ is the feature vector expression of the i-th segment of the k-th type of kinematic segment; and μ_k is the feature vector expression of the i-th segment of the k-th type of kinematic segment.

In order to avoid selecting of kinematic segments with ambiguous categories, when splicing kinematic segments of each category, segments that meet the duration requirements and are closer to the centroid is selected. There is a total of 12 candidate driving cycles.

1.4.2 Error analysis and verification of driving cycles

After the set of candidate driving cycles is constructed, the error analysis is also required. On the one hand, it is to select the driving cycle with the smallest error from the candidate driving cycles as the final driving cycle, on the other hand, it is to verify the accuracy of the final driving cycle. The method of error analysis is to calculate the 21 significant indicators of each synthetic driving cycle, and compare the calculated indicators with the corresponding values of the overall data, and calculate the average error rate between the candidate driving cycles and the overall data. The results are shown in the table 8. There is no large deviation between the index values of the 12 candidate driving cycles and the overall data, and the average error is between 5% and 7%. It shows that the constructed driving cycles have a high degree of fit with the actual driving cycle. A driving cycle with the smallest error rate was selected as the representative driving cycle, and its average error rate was 5.53%.

Table 8 Error analysis of candidate operating conditions

Param	1	2	3	4	5	6	7	8	9	10	11	12	Total data
T_i	0.22	0.18	0.20	0.17	0.20	0.16	0.21	0.17	0.19	0.16	0.19	0.15	0.17
T_a	0.35	0.37	0.37	0.38	0.36	0.38	0.36	0.38	0.38	0.39	0.37	0.39	0.36
T_d	0.31	0.32	0.31	0.32	0.32	0.33	0.31	0.32	0.32	0.33	0.32	0.33	0.33
T_e	0.12	0.13	0.12	0.13	0.12	0.13	0.12	0.13	0.11	0.12	0.12	0.13	0.14
V_m	34.3	36.9	34.2	36.7	34.8	37.0	33.7	36.4	33.8	36.2	34.3	36.5	36.2
V_{mr}	43.0	44.3	42.2	43.5	42.6	43.7	41.9	43.3	41.2	42.6	41.7	42.9	43.0
V_s	22.7	21.6	22.0	21.1	21.8	20.9	22.3	21.4	21.7	21.0	21.6	20.8	24.7
A_m	0.53	0.51	0.53	0.52	0.53	0.52	0.53	0.51	0.53	0.51	0.53	0.51	0.54
A_s	0.42	0.43	0.42	0.43	0.42	0.43	0.42	0.42	0.41	0.42	0.42	0.42	0.42
D_m	0.59	0.58	0.61	0.60	0.58	0.58	0.58	0.58	0.60	0.59	0.57	0.57	0.57

Table 8 (Continued)

Param	1	2	3	4	5	6	7	8	9	10	11	12	Total data
D_s	0.45	0.45	0.46	0.45	0.45	0.45	0.46	0.45	0.46	0.46	0.45	0.45	0.47
T_f	0.73	0.74	0.74	0.74	0.74	0.73	0.73	0.73	0.74	0.74	0.73	0.73	0.71
T_b	0.26	0.25	0.25	0.25	0.26	0.26	0.26	0.26	0.25	0.25	0.26	0.26	0.28
I_{fm}	31.6	33.9	33.8	35.5	34.2	35.7	31.0	33.3	33.2	34.9	33.6	35.1	33.7
I_{fs}	34.6	34.3	35.2	34.8	34.7	34.4	34.0	33.9	34.7	34.4	34.2	34.0	36.9
Ib_m	21.8	22.5	21.8	22.5	21.3	22.0	21.5	22.2	21.5	22.2	21.1	21.7	21.0
Ib_s	18.1	17.8	18.1	17.8	17.3	17.2	17.8	17.6	17.8	17.6	17.1	17.0	19.5
IA_m	19.0	19.7	19.1	19.7	18.6	19.3	18.3	19.1	18.5	19.2	18.0	18.8	16.2
IA_s	23.5	23.3	23.1	23.0	22.7	22.7	22.9	22.9	22.7	22.7	22.2	22.3	23.0
ID_m	21.2	22.7	21.6	23.0	21.1	22.6	20.8	22.4	21.3	22.7	20.9	22.2	18.7
ID_s	27.9	27.3	27.7	27.0	27.0	26.5	27.5	26.9	27.3	26.8	26.6	26.2	27.6
Error rate (%)	6.19	6.51	6.44	7.0	5.53	6.54	6.47	6.34	6.91	6.95	5.99	6.44	—

1.5 Driving cycle output

The representative driving cycle is screened out through the error analysis, and the duration of the representative driving cycle was 1 589 s, where the time of low velocity, medium and low velocity, medium and high velocity, and high velocity are 189, 257, 853 s and 290 s respectively. According to the vehicle velocity and battery current of the driving cycle, the vehicle driving cycle curve and the battery driving cycle curve are respectively drawn.

1.5.1 Vehicle driving cycle curve

The vehicle driving cycle of Chongqing pure electric vehicle in the mountain environment is shown in Figure 7.

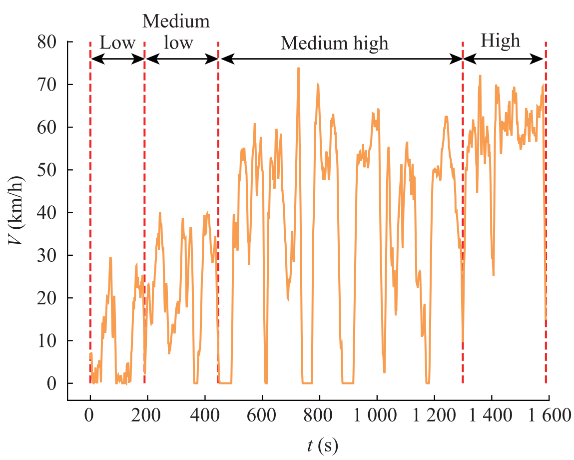

Fig. 7 Velocity-time curve of Chongqing battery electric vehicle

1.5.2 Battery driving cycle curve

The battery driving cycle curve of Chongqing pure electric vehicle in mountainous environment is shown in Figure 8.

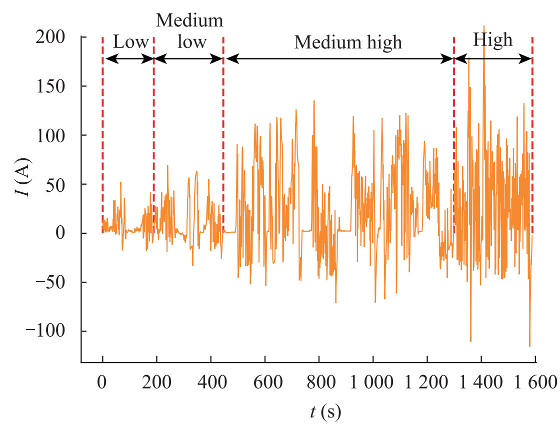

Fig. 8 Current-time curve of Chongqing battery electric vehicle

2 Comparative analysis

Using the above method of constructing driving cycle, the vehicle driving cycle and battery driving cycle of Beijing PEV are constructed for the same model in Beijing. Firstly, the vehicle driving cycle of Chongqing and Beijing are compared with NEDC, WLTC, CLTC-P, the main indicators are shown in Table 9. Then battery driving cycle of PEV in Chongqing and Beijing are compared, and the main indicators are shown in Table 10.

Table 9 Comparison of velocity-time curve of Chongqing with others

Param	Vehicle driving cycle of Chongqing	Vehicle driving cycle of Beijing	NEDC	WLTC	CLTC-P
T(s)	1 589	2 035	1 180	1 800	1 800
S(m)	15.36	19.67	11.00	23.20	14.48
V_m(km/h)	34.80	34.80	33.60	46.40	28.96
V_{mr}(km/h)	42.60	40.10	43.50	53.20	37.18
A_m(m/s^2)	0.53	0.54	0.53	0.53	0.45
D_m(m/s^2)	−0.58	−0.52	−0.75	−0.58	−0.49
T_a(%)	36.00	36.50	23.30	30.90	28.61
T_d(%)	32.00	36.00	16.60	28.60	26.44
T_e(%)	12.00	13.50	37.50	27.80	22.83
T_i(%)	20.00	14.00	22.60	12.70	22.12

Table 10 Comparison of current-time curve of Chongqing with others

Param	T(s)	I_{fm} (A)	Ib_m (A)	IA_m (A/s)	ID_m (A/s)	T_f (%)	T_b (%)
Battery driving cycle of Chongqing	1 589	34.20	21.30	18.60	21.10	74	26
Battery driving cycle of Beijing	2 035	29.60	17.90	15.90	18.80	71	29

The comparative analysis shows that: the values of average vehicle velocity, average running velocity and average acceleration in vehicle driving cycle are similar to that in NEDC, but the difference is obvious in other features; the values of features in vehicle driving cycle are obviously different to that in WLTC except for the average acceleration and average deceleration; compared with CLTC-P, there are significant differences in each indicators. From the comparison of the driving cycle of PEV in Chongqing and Beijing, it can be seen that the average deceleration in Chongqing is 11.5% larger than that in Beijing, and the proportion of deceleration time is smaller than that of Beijing, and the proportion of idle time is larger than that of Beijing. From the perspective of battery driving cycle, it is found that the values of features in Chongqing are larger than that in Beijing except the value of energy recovery proportion, and there are obvious differences caused by the geographical environment.

3 Conclusion

In this paper, the improved short-stroke method is used to decompose the kinematic segments, and the battery characteristic indicators are added. Principal component analysis and K-means++ cluster analysis are used to construct the vehicle driving cycles and battery driving cycles of the pure electric vehicle in the mountain environment by weighted combination.

The average error between the driving cycle and the actual driving data is 5.53%. This indicates that the driving cycle accurately reflects the actual driving patterns of PEV. Through comparative analysis, it is verified that there are significant differences between the pure electric vehicle driving cycles constructed in this paper and the classic ones. By constructing the pure electric vehicle driving cycle in Beijing for comparison, it is verified that the mountain environment has an influence on the driving cycle, and the validity of the driving cycle constructed in this paper is proved.

The driving cycle of PEV in the mountain environment have the characteristics of less uniform time, high idling time, greater deceleration than non-mountain environments. The driving cycle of pev in mountainous environments exhibits several distinct characteristics. Compared to non-mountainous environments, they have less uniform time distribution, higher idling time, greater deceleration intensity but shorter deceleration duration, lower battery discharge process efficiency, and moderate velocity. By constructing driving cycles for pure electric vehicles in diverse geographical environments, we can not only analyze their specific characteristics but also verify the distinct differences between mountainous and non-mountainous environments.

Declaration of competing interest

The authors have no competing interests to declare that are relevant to the content of this article.

References

[1] HUERTAS J I, DÍAZ J, CORDERO D, et al. A New Methodology to Determine Typical Driving Cycles for The Design of Vehicles Power Trains [J]. Springer Paris,

2018, 12 (1): 319-326.

[2] ZHANG Jian-wei, LI Meng-liang, AI Guo-he, et al. A Study on the Features of Existing Typical Vehicle Driving Cycles [J]. Automotive Engineering, 2005 (2): 220-224, 245. (in Chinese)

[3] CAI E, LI Yang-yang, LI Chun-ming, et al. Research on Synthetic Technique of Driving Cycle in Xi'an Based on K-means Clustering [J]. Automobile Technology, 2015 (8): 33-36. (in Chinese)

[4] XU Ting, CUI Shi-chao, LIU Ming, et al. Study on Construction Method of Driving Cycle of Passenger Vehicle in Plateau Mountainous Area [J]. Journal of Highway and Transportation Research and Development, 2021, 38 (2): 117-124. (in Chinese)

[5] SUN Jun, FANG Tao, ZHANG Bing-li, et al. Construction of Hefei Electric Buses Driving Cycle Based on Improved K-Means Clustering [J]. Automobile Technology, 2020 (8): 56-62. (in Chinese)

[6] LIU Yu, WU Zhi-xin, LI Meng-liang, et al. Development of China Light-duty Passenger Car Test Cycle [J]. Journal of Transportation Systems Engineering and Information Technology, 2020, 20 (3): 233-240. (in Chinese)

[7] GB/T 38146.1—2019, China Automotive Test Cycle—Part 1: Light-duty Vehicles [S]. (in Chinese)

[8] TONG H Y. Development of a Driving Cycle for a Super Capacitor Electric Bus Route in Hong Kong [J]. Sustainable Cities and Society, 2019, 48 (7): 233-240.

[9] HU Zheng-yun. Study on Construction Method of Urban Driving Cycle of Passenger Vehicles [J]. Journal of Highway and Transportation Research and Development, 2019, 36 (11): 142-150. (in Chinese)

[10] WANG WEN-qi, GAO Guang-kuo, WANG Zi-jian, et al. A Method for Constructing Automobile Operation Condition [J]. Journal of Highway and Transportation Research and Development, 2020, 37 (9): 128-138. (in Chinese)

[11] HU Zhi-yuan, QIN Yan, TAN Pei-qiang, et al. Large-sampled-based Car-driving Cycle in Shanghai City [J]. Journal of Tongji University (Natural Science), 2015, 43 (10): 1523-1527. (in Chinese)

[12] GAO Chi. Grasp the Situation, Focus on Transformation, Lead Innovation, Recording the 2020 China Electric Vehicle Hundreds Conference Forum [J]. Automobile & Parts, 2020 (3): 26-29. (in Chinese)

[13] YU Man, ZHAO Wei-hua, WU Ling, et al. Working Condition of Electric Vehicle Based on K-Mean Clustering and Support Vector Machine [J]. Journal of Chongqing Jiaotong University (Natural Science), 2021, 40 (5): 129-139. (in Chinese)

[14] KUI Hai-xia, SONG Ruo-yang, LAN Hai-chao, et al. Research on Construction Method of Electric Vehicle Urban Driving Conditions [J]. Automobile Applied Technology, 2020, 45 (22): 10-13. (in Chinese)

[15] LI Yao-hua, LIU Peng, YANG Wei, et al. Research on Xi'an Pure Electric Bus Driving Cycle [J]. China Sciencepaper, 2016, 11 (7): 754-759. (in Chinese)

[16] XU Xiao-jun, LI Jun, LIU Yu, et al. The Development of Electric Vehicles Urban Driving Cycle [J]. Science Technology and Engineering, 2017, 17 (35): 330-336. (in Chinese)

[17] PAN Deng. Study on Urban Driving Cycle Construction and Its Multi-scale Prediction for Hybrid Electric Vehicles [D]. Beijing: Beijing Institute of Technology, 2015. (in Chinese)

[18] MA Zhi-xiong, LI Meng-liang, ZHU Xi-chan, et al. Study of the Methodology for Car Driving Cycle Development [J]. Journal of Wuhan University of Technology (Information & Management Engineering), 2004 (3): 182-184, 188. (in Chinese)